Acta Crystallographica Section A
Foundations of Crystallography
ISSN 0108-7673

Received 14 March 2007
Accepted 2 May 2007

Correlated grain-boundary distributions in two-dimensional networks

Jeremy K. Mason and Christopher A. Schuh*

Department of Materials Science and Engineering, Massachusetts Institute of Technology, 77 Massachusetts Avenue, Cambridge, MA 02139, USA. Correspondence e-mail: schuh@mit.edu

In polycrystals, there are spatial correlations in grain-boundary species, even in the absence of correlations in the grain orientations, due to the need for crystallographic consistency among misorientations. Although this consistency requirement substantially influences the connectivity of grain-boundary networks, the nature of the resulting correlations are generally only appreciated in an empirical sense. Here a rigorous treatment of this problem is presented for a model two-dimensional polycrystal with uncorrelated grain orientations or, equivalently, a cross section through a three-dimensional polycrystal in which each grain shares a common crystallographic direction normal to the plane of the network. The distribution of misorientations θ, boundary inclinations φ and the joint distribution of misorientations about a triple junction are derived for arbitrary crystal symmetry and orientation distribution functions of the grains. From these, general analytical solutions for the fraction of low-angle boundaries and the triple-junction distributions within the same subset of systems are found. The results agree with existing analysis of a few specific cases in the literature but present a significant generalization.

1. Introduction

The properties and behaviour of polycrystalline materials are strongly influenced by crystallographic elements of their microstructure. Generally, the more information that a particular function provides about the microstructure, the more difficult is its measurement and relation to actual material behaviour. As a result, it is a continuing challenge to express the microstructure in terms of a simple function that still captures enough of the relevant crystallographic information to allow reasonable predictions of material properties. This is especially true for the broad range of properties that depend on the character of grain boundaries, for which the classical orientation distribution function (Roe, 1965, 1966; Haessner *et al.*, 1983; Bunge, 1993) does not directly apply. Many of the physical properties of grain boundaries appear to be principally related to their misorientation (Handscomb, 1957; Mackenzie & Thomson, 1957; Mackenzie, 1958, 1964; Grimmer, 1974; Warrington & Boon, 1975; Grimmer, 1979, 1980; Haessner *et al.*, 1983; Zhao & Adams, 1988; Adams *et al.*, 1990; Morawiec, 1995; Morawiec & Field, 1996), and determination of the distribution of this quantity is often the focus of grain-boundary characterization. The coincidence site lattice (CSL) theory provides a specific model to understand the relationship connecting misorientation to physical properties, and is frequently used in the literature (Brandon, 1966; Warrington & Boon, 1975). A more refined analysis of boundary properties reveals a dependence on the orientation of the interface as well; interest in the distributions of boundary normals (Hilliard, 1962; Philofsky & Hilliard, 1969; Adams & Field, 1992), the indices of the crystallographic planes meeting at an internal interface (Saylor *et al.*, 2003*a*,*b*; Saylor, El Dasher, Rollett & Rohrer, 2004; Saylor, El Dasher, Pang *et al.*, 2004; Saylor, El Dasher, Sano & Rohrer, 2004), and joint distributions of the misorientation and plane of a boundary (Adams, 1986; Zhao *et al.*, 1988; Morris *et al.*, 1988) is increasing.

While these distributions provide significant information about individual grain boundaries in a microstructure, a number of investigations suggest that this description is insufficient for certain applications. For example, the connection between orientation and misorientation distributions is ambiguous; materials sharing a single orientation distribution function may exhibit different CSL misorientation fractions (Gertsman *et al.*, 1992; Pan & Adams, 1994). Some findings suggest that this is due to neglect of orientation correlations of adjoining grains (Zhao *et al.*, 1988; Gertsman *et al.*, 1992; Adams, 1993; Pan & Adams, 1994), or to differences in the connection length for boundaries of a distinct type (Adams *et al.*, 1993). The development of theories to satisfactorily explain these variations in grain-boundary character necessarily involves structures more complicated than a single grain boundary; any analysis must begin with the structures within which the observed correlations occur. Since a triple junction is the smallest segment of the boundary network more inclusive than a single grain boundary, this structure is a natural candidate. Analyses of triple junctions within the CSL theory reveal that the granular nature of the material sharply

constrains the sets of misorientations allowed at these junctions (Miyazawa, Iwasaki *et al.*, 1996; Miyazawa, Ito & Ishida, 1996; Minich *et al.*, 2002; Frary & Schuh, 2003*a*; Reed & Kumar, 2006). In other words, there are necessary correlations in the misorientation distributions, even when the grain orientations are completely uncorrelated. The experimental importance of this constraint upon the properties of polycrystals was first emphasized by Kumar *et al.* (2000). Gertsman presented a particularly rigorous analysis of these correlations for ideal CSL misorientations, and further extended his analysis to higher-order structures including quadruple nodes (Gertsman, 2001*a*,*b*, 2002). Alternatively, triple junctions and their effect on the connectivity of boundaries in the network have been investigated using percolation theory (Frary & Schuh, 2003*b*; Schuh, Kumar & King, 2003*a*,*b*; Schuh, Minich & Kumar, 2003; Frary & Schuh, 2004; Van Siclen, 2006), although studies on correlations in structures more complicated than triple junctions remain, for the most part, empirical observations (Frary & Schuh, 2005*a*,*b*; Schuh & Frary, 2006).

The purpose of this paper is to develop a methodology for analysing correlations, arising purely from the granular nature of polycrystalline materials, in the quantities that uniquely specify the states of grain boundaries. Our approach differs from the pertinent existing literature described above in the sense that we do not classify the boundaries (*e.g.* by the CSL model) prior to examining the strength of the correlations. Rather, we perform classification as a subsequent step, since boundary classification reduces the available information and thereby obscures the effects of correlations. This further allows our results to be interpreted using classification schemes other than the one used herein. The approach is worked out in detail for an arbitrary two-dimensional polycrystal with no spatial correlation in grain orientations; extension to the three-dimensional analogue will be addressed in future research.

2. Definition of the system

Our system consists of a two-dimensional polycrystal, in which the orientation of each grain is fully specified by a single rotation in the plane, through an angle ω relative to a fixed reference orientation. This construct also applies to a cross section through a three-dimensional polycrystal in which each grain shares a common crystallographic direction **n** normal to the plane of the network, with ω the rotation about **n**. The area orientation distribution function is, for a uniform grain size, identical to the distribution of orientations of the crystallites (Bunge, 1993), and expresses the probability that the orientation of a single grain is given by ω. Similarly, the distribution in the orientations of the boundary planes is specified as a function of the angle ϕ, measured with respect to the same reference orientation. Assuming that there are no correlations among grain orientations and none relating the grain orientations to the boundary normal, this information is sufficient to determine the distribution function describing the types of grain boundaries present in the material. While a two-dimensional polycrystal is a significant simplification from the three-dimensional polycrystals typically studied in practice, the majority of the literature on grain-boundary correlations currently focuses on grain-boundary types in two-dimensional cross sections. The present treatment therefore allows ready comparison with some existing literature and, furthermore, is expected to generalize to the three-dimensional case.

We represent the orientation distribution function $f(\omega)$ as a Fourier series with periodicity $\omega_s = 2\pi/k$, where an axis of k-fold rotational symmetry coincides with the **n** direction. This yields, for an arbitrary distribution function of the appropriate symmetry,

$$f(\omega) = \frac{1}{\omega_s} + \sum_{n=1}^{\infty} a_n \cos(kn\omega) + b_n \sin(kn\omega), \qquad (1)$$

where the Fourier coefficients a_n and b_n prescribe the details of the preferred orientation. Notice that $f(\omega)$ is normalized over $-\omega_s/2 \leq \omega < \omega_s/2$, since this range contains all unique crystallite orientations. Meanwhile, we shall constrain our attention to simple systems based on a single triple junction schematically represented in Fig. 1, with the grains and boundaries labelled A, B and C in the manner depicted. Grain orientations and grain-boundary descriptors will be labelled with these subscripts in some cases, *e.g.* ω_A denotes the orientation of grain A.

A single boundary is completely specified by the rotations ω and ω' of the adjacent grains and by the inclination ϕ, each measured with respect to the reference orientation. Although ω is a natural variable of the orientation distribution function describing the state of the grains, it is not a clear descriptor for a grain boundary. Since the properties of a grain boundary must remain invariant under an arbitrary rotation of the material, the natural quantities to describe a grain boundary

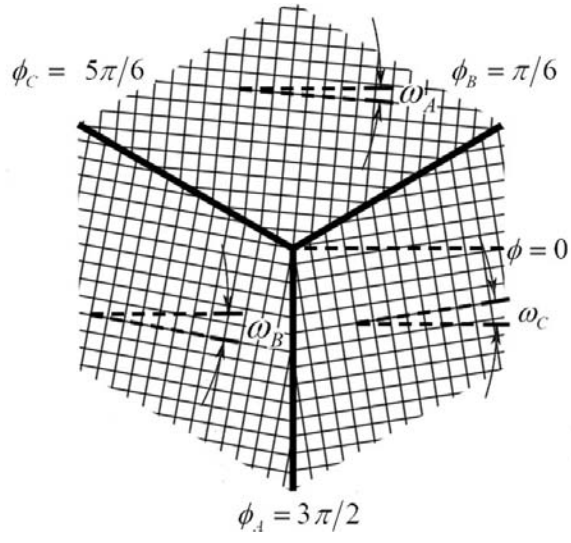

Figure 1
Representative triple junction depicting the physical significance of the quantities ω and ϕ. Grain A is rotated by the angle ω_A and is located opposite the boundary with orientation ϕ_A; a similar geometry applies for grains B and C.

must be defined in the local crystal frame. The misorientation of adjoining grains is explicitly given by

$$\theta = \omega' - \omega. \tag{2}$$

Meanwhile, following the notation of Read & Shockley (1950), we define the orientation φ of the boundary plane in a manner that shares the misorientation equally between the grains, or

$$\varphi = \phi - \frac{\omega' + \omega}{2}. \tag{3}$$

These relationships may be derived from examination of Fig. 2, which depicts a single boundary defined relative to the external and local reference frames.

Each grain orientation ω is symmetrically equivalent to the value $\omega + n\omega_s$ for any integer value of n, and similarly ω' is symmetrically equivalent to the value $\omega' + m\omega_s$ for any integer value of m. Then, according to equation (2), θ is symmetrically equivalent to $\theta + \omega_s(m - n)$, and the distribution of θ displays a periodicity of ω_s. Similarly, φ is symmetrically equivalent to $\varphi - \omega_s(m + n)/2$, and the distribution of φ displays a periodicity of $\omega_s/2$. However, when θ and φ refer to the same boundary and share values for the indices m and n, the periodicities change to $2\omega_s$ and ω_s, respectively. Since simple distributions, *e.g.* of the misorientation alone, display the periodicity corresponding to the first case, θ and φ are *defined* to fall within the ranges $-\omega_s/2 \leq \theta < \omega_s/2$ and $-\omega_s/4 + \phi \leq \varphi < \omega_s/4 + \phi$. As we shall see, in some cases this necessitates the application of further symmetries in order to enforce the required periodicity on joint distribution functions.

Crystallographic constraints impact the local grain-boundary statistics only when considering the values of θ and φ for multiple boundaries simultaneously; in other words, the granular crystalline nature of the material generates spatial correlations in grain-boundary character, despite the absence of correlations in grain orientations. For example, consider the grains and boundaries around a triple junction, as appears in Fig. 3. The orientations ω of the three grains are specified independently. θ and φ for each boundary depend on the orientations of the adjoining grains or, alternatively, the orientation of a single grain influences the type of each of the adjoining boundaries. Therefore, the θ and φ for multiple boundaries may not be considered independently. Since these quantities uniquely specify the state of a grain boundary, and our purpose is to examine correlations in boundary character arising from the granular crystalline nature of the material, the remainder of this paper is devoted to finding distributions of and correlations among the θ and φ given a set of grain orientations ω, each independently distributed according to the arbitrary orientation distribution function $f(\omega)$. The

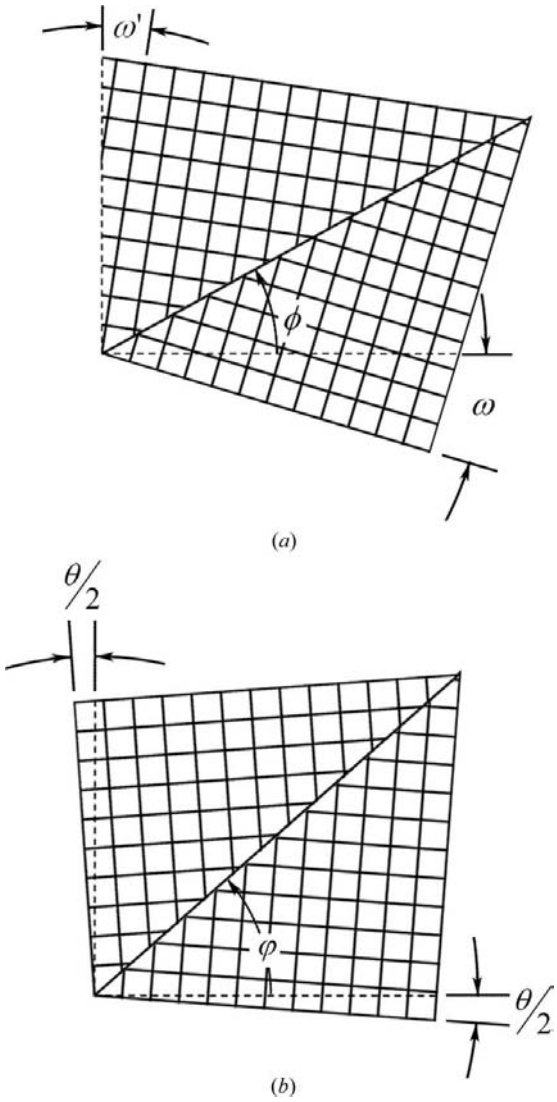

Figure 2
Comparison of the quantities used to define the state of a grain boundary. A single boundary is depicted in terms of (*a*) ω, ω' and ϕ and (*b*) θ and φ. Notice that in (*b*) the grains share the misorientation equally, resulting from a rotation of the system in (*a*).

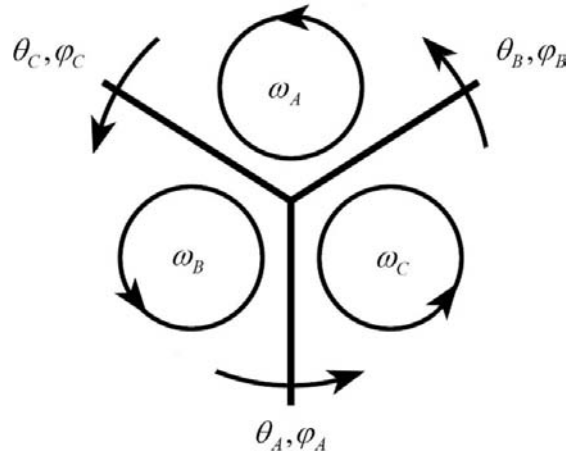

Figure 3
Labelling scheme for the grain rotations ω and the quantities θ and φ around a triple junction. The misorientations θ are the rotations that bring the grain at the tail of the arrow into coincidence with the grain at the head. Our labelling scheme differs in sense from some similar examples in the literature (Frary & Schuh, 2004).

procedure for finding a joint distribution of a set of the quantities θ and φ is as follows.

(i) Construct the function

$$F(\boldsymbol{\omega}) = f(\omega_1)f(\omega_2)\ldots f(\omega_n) \tag{4}$$

to provide the joint distribution of rotations ω_j of each of the n grains involved in the problem, where $\boldsymbol{\omega}$ is a vector quantity containing the n ω_j as elements. For example, $n = 2$ for a single grain boundary and $n = 3$ for a triple junction. Notice that this equation expressly forbids the introduction of correlations in grain orientations.

(ii) State the equations relating the known grain rotations ω_j to the grain-boundary character parameters; these desired quantities are called y_i, with each of the y_i denoting either a θ or a φ as in equations (2) and (3). Examination of the definitions of θ and φ reveals that these are linear or affine functions of the grain rotations, suggesting a compact expression for the transformation equations in the form

$$\mathbf{y} = \boldsymbol{A}\boldsymbol{\omega}, \tag{5}$$

where $\mathbf{y}$ is a vector quantity containing the m y_i as elements and $\boldsymbol{A}$ is the m by n transformation matrix. Situations where $\boldsymbol{A}$ is affine will require the modification of $\boldsymbol{\omega}$ and $\mathbf{y}$ to conform with the use of homogeneous coordinates by appending a constant term to these vectors.

(iii) Determine the equations of the inverse transformation, relating the y_i to the ω_j. Provided the transformation matrix $\boldsymbol{A}$ is invertible, the equation containing the inverse transformation equations is

$$\boldsymbol{\omega} = \boldsymbol{A}^{-1}\mathbf{y}. \tag{6}$$

When the matrix $\boldsymbol{A}$ is not invertible, $\boldsymbol{A}$ must be decomposed by singular-value decomposition (see *e.g.* Strang, 2006), and the non-invertible component removed by integration.

(iv) Substitute the expressions for the ω_j in terms of the y_i into the joint probability distribution of the ω_j in equation (4) to find the joint probability distribution of the desired quantities y_i. This amounts to a transformation of space, from one spanned by the ω_j to one spanned by the y_i, in which a single probability distribution function is embedded. Since this transformation generally includes a stretching component, the transformed probability density function must be multiplied by an appropriate factor to remain normalized; in situations where $\boldsymbol{A}$ is invertible, this factor is the magnitude of the determinant of $\boldsymbol{A}^{-1}$. Otherwise, the necessary multiplicative factor is found by multiplying the inverses of the singular values of $\boldsymbol{A}$.

(v) Adjust the distribution function to account for symmetry defined to be present in the distributions of the y_i that is not captured by the inherent periodicity of the ω_j. Generally, this requires summing the derived distribution function with an equivalent distribution function shifted by an appropriate distance in the $\mathbf{y}$ space.

Since the full transformation procedure is often quite involved, a series of examples follows.

3. Distribution functions for a single boundary

As defined above, a single boundary is uniquely specified by a pair of values θ and φ; the distribution function completely characterizing a single boundary is given by the joint probability distribution function of these quantities. We perform this derivation for the boundary type described by θ_A and φ_A, which depend exclusively on ω_B and ω_C, as indicated in Fig. 3.

3.1. Joint distribution of θ and φ

Step (i) is to construct the joint distribution function for ω_B and ω_C; reference to equations (1) and (4) indicates that the relevant distribution function of the grain rotations is

$$\begin{aligned} F(\omega_B, \omega_C) = \frac{1}{\omega_s^2} + \frac{1}{\omega_s}\Bigg\{ & \sum_{n=1}^{\infty} a_n[\cos(kn\omega_B) + \cos(kn\omega_C)] \\ & + b_n[\sin(kn\omega_B) + \sin(kn\omega_C)]\Bigg\} \\ & + \Bigg\{ \sum_{m=1}^{\infty}\sum_{n=1}^{\infty} [a_m \cos(km\omega_B) + b_m \sin(km\omega_B)] \\ & \times [a_n \cos(kn\omega_C) + b_n \sin(kn\omega_C)]\Bigg\}. \end{aligned} \tag{7}$$

To execute step (ii), we refer to equations (2) and (3), which indicate that the desired quantities may be expressed in terms of the grain rotations as

$$\begin{pmatrix} \theta_A \\ \varphi_A \\ 1 \end{pmatrix} = \begin{pmatrix} -1 & 1 & 0 \\ -1/2 & -1/2 & \phi_A \\ 0 & 0 & 1 \end{pmatrix} \begin{pmatrix} \omega_B \\ \omega_C \\ 1 \end{pmatrix}. \tag{8}$$

Since the expression for φ_A includes a constant term, the transformation $\boldsymbol{A}$ contains a translational component; $\boldsymbol{A}$ is therefore affine, and is expressed in matrix form using homogeneous coordinates. Since $\boldsymbol{A}$ is invertible, step (iii) is straightforward:

$$\begin{pmatrix} -1/2 & -1 & \phi_A \\ 1/2 & -1 & \phi_A \\ 0 & 0 & 1 \end{pmatrix} \begin{pmatrix} \theta_A \\ \varphi_A \\ 1 \end{pmatrix} = \begin{pmatrix} \omega_B \\ \omega_C \\ 1 \end{pmatrix}, \tag{9}$$

from which we obtain $\omega_B = -\theta_A/2 - \varphi_A + \phi_A$ and $\omega_C = \theta_A/2 - \varphi_A + \phi_A$. Substitution of these equalities into equation (7) and multiplication by the magnitude of the determinant of $\boldsymbol{A}^{-1}$ in equation (9) completes step (iv). The joint distribution of θ and φ is

$$F(\theta,\varphi)=\frac{1}{\omega_s^2}+\frac{2}{\omega_s}\Bigg(\sum_{n=1}^{\infty}\cos\left(\frac{k}{2}n\theta\right)\{a_n\cos[kn(\varphi-\phi)]-b_n\sin[kn(\varphi-\phi)]\}\Bigg)+\Bigg(\sum_{m=1}^{\infty}\sum_{n=1}^{\infty}\Bigg\{a_m\cos\left[km\left(\frac{\theta}{2}+\varphi-\phi\right)\right]-b_m\sin\left[km\left(\frac{\theta}{2}+\varphi-\phi\right)\right]\Bigg\}\times\Bigg\{a_n\cos\left[kn\left(\frac{\theta}{2}-\varphi+\phi\right)\right]+b_n\sin\left[kn\left(\frac{\theta}{2}-\varphi+\phi\right)\right]\Bigg\}\Bigg),\quad(10)$$

where the subscript A has been dropped, since this result applies to any boundary with an arbitrary inclination ϕ in the external reference frame.

Recall that the periodicity of ω implies the symmetric equivalence of θ with $\theta+\omega_s(m-n)$, and of φ with $\varphi-\omega_s(m+n)/2$. If these periodicities are independent of one another (*i.e.* if m and n are independent), the symmetries of the system can be represented by the lattice of symmetrically equivalent points displayed in Fig. 4(*a*), which is consistent with the required boundary conditions on θ and φ. However, in the present case θ and φ refer to the same grain boundary, and the indices m and n are shared. Therefore, the symmetry of equation (10) is represented by the lattice in Fig. 4(*b*); observe that this lattice misses some of the required symmetries in the definition of θ and φ, *i.e.* Fig. 4(*b*) is of lower symmetry than is Fig. 4(*a*). Therefore, equation (10) must be modified to incorporate the required symmetries. Examination of these figures indicates that the lattice in Fig. 4(*a*) may be constructed by combining the lattice in Fig. 4(*b*) with the equivalent lattice shifted in the θ direction by ω_s or in the φ direction by $\omega_s/2$; this leads to the equation

$$\mathscr{F}(\theta,\varphi)=F(\theta,\varphi)+F(\theta-\omega_s,\varphi)=F(\theta,\varphi)+F(\theta,\varphi-\omega_s/2),\quad(11)$$

where the symbol $\mathscr{F}$ denotes the final distribution function with the proper symmetry that is consistent with the specified periodicities. The conversion from the function F to $\mathscr{F}$ completes step (v) of the derivation.

3.2. Individual distributions in θ and φ

Once the function $\mathscr{F}$ is found, relevant subdistributions may be readily determined. For example, the joint distribution function of θ and φ contains information specifying the distribution functions for θ and φ separately; these separate distributions are found by integrating out the dependence on the other variable. This may be done using either F or $\mathscr{F}$, which return identical results provided that the integral is performed over one period of the distribution in the dimension of the variable to be removed. While $\mathscr{F}$ is consistent with the preceding definitions of θ and φ, the integration is often simpler in F due to the nature of the trigonometric terms present.

The probability density function describing the distribution of misorientations θ is given by

$$\begin{aligned}\mathscr{F}(\theta)&=\int_{-\omega_s/4+\phi}^{\omega_s/4+\phi}\mathscr{F}(\theta,\varphi)\,\mathrm{d}\varphi\\&=\tfrac{1}{2}\int_{-\omega_s/2+\phi}^{\omega_s/2+\phi}F(\theta,\varphi)+F(\theta-\omega_s,\varphi)\,\mathrm{d}\varphi\\&=\int_{-\omega_s/2+\phi}^{\omega_s/2+\phi}F(\theta,\varphi)\,\mathrm{d}\varphi.\end{aligned}\quad(12)$$

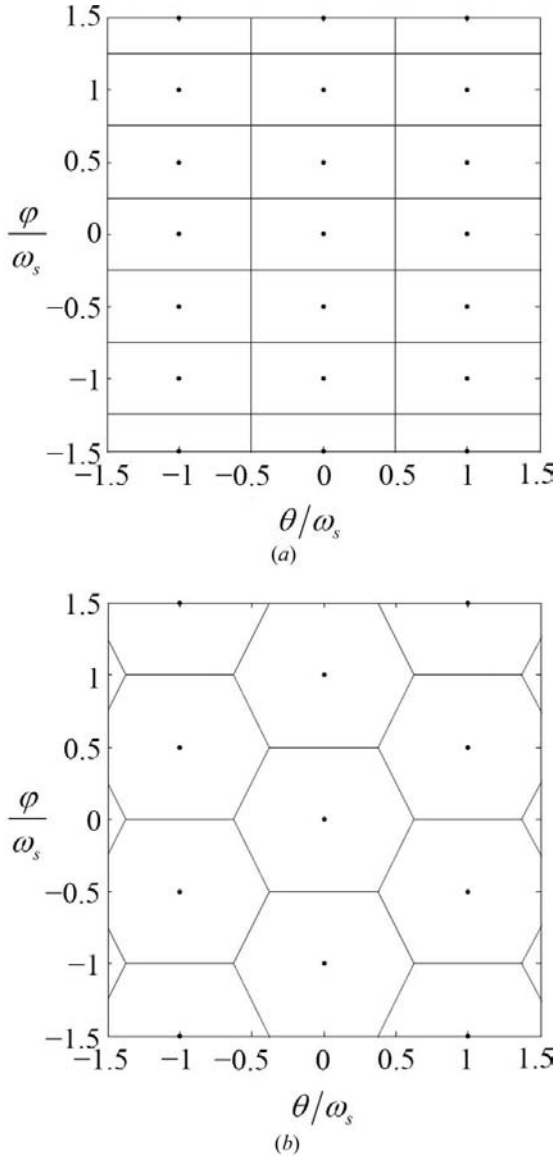

Figure 4
Lattices of symmetrically equivalent points and corresponding unit cells for θ and φ at a single grain boundary. (*a*) θ and φ display independent periodicities of ω_s and $\omega_s/2$, respectively, resulting in a rectangular lattice and simply described boundaries. (*b*) θ and φ display joint periodicities, leading to a sparser lattice, an extended range of unique quantity pairs and more complicated boundaries.

The trigonometric terms in this integral either vanish for all values of the indices m and n or evaluate to constants for $m = n$ and vanish for other values, according to the relations provided in Appendix A. With simplification, this integral returns

$$\mathscr{F}(\theta) = \frac{1}{\omega_s} + \frac{\omega_s}{2}\sum_{n=1}^{\infty}(a_n^2 + b_n^2)\cos(kn\theta) \tag{13}$$

for the distribution of misorientation angles in the boundary network. Similarly, the distribution of boundary plane normals φ is determined as

$$\begin{aligned}\mathscr{F}(\varphi) &= \int_{-\omega_s/2}^{\omega_s/2} \mathscr{F}(\theta,\varphi)\,\mathrm{d}\theta \\ &= \tfrac{1}{2}\int_{-\omega_s}^{\omega_s} F(\theta,\varphi) + F(\theta,\varphi-\omega_s/2)\,\mathrm{d}\theta \\ &= \int_{-\omega_s}^{\omega_s} F(\theta,\varphi)\,\mathrm{d}\theta. \end{aligned}\tag{14}$$

Following simplification with reference to Appendix A, this yields the distribution function

$$\begin{aligned}\mathscr{F}(\varphi) = \frac{2}{\omega_s} + \omega_s\sum_{n=1}^{\infty}\{&(a_n^2 - b_n^2)\cos[2kn(\varphi-\phi)] \\ &- 2a_nb_n\sin[2kn(\varphi-\phi)]\}.\end{aligned}\tag{15}$$

4. Triple-junction misorientation distribution

Within the literature, studies of the effects of crystallographic constraints on grain-boundary networks frequently concentrate on the character and influence of the constraints on boundaries joining at triple junctions (Miyazawa, Iwasaki *et al.*, 1996; Miyazawa, Ito & Ishida, 1996; Kumar *et al.*, 2000; Gertsman, 2001*a*,*b*; Kumar *et al.*, 2002; Gertsman, 2002; Minich *et al.*, 2002; Frary & Schuh, 2003*a*,*b*; Schuh, Kumar & King, 2003*a*,*b*; Schuh, Minich & Kumar, 2003; Frary & Schuh, 2004, 2005*a*,*b*; Schuh *et al.*, 2005; Van Siclen, 2006). The reason for this is probably related to the increasing difficulty of analysis with the extent of the boundary structure considered, and to the decrease in strength of the correlations in boundary character with the spatial separation of the boundaries (Schuh & Frary, 2006). Therefore, analyses of triple junctions provide descriptions of some of the more mathematically accessible correlations, and substantial information about the nature of the network. The analysis of correlations in grain-boundary character around a triple junction is hence not only of practical interest but provides an opportunity to compare the results derived using our method to those appearing in the literature. For the sake of simplicity, the joint distribution function of the three misorientations θ_A, θ_B and θ_C is determined, without consideration of the boundary-plane inclinations.

Reference to Fig. 3 reveals that the misorientations of the three boundaries around a triple junction depend on the rotations of the three grains meeting at the triple junction; that is, θ_A, θ_B and θ_C depend upon ω_A, ω_B and ω_C. The joint distribution function constructed in step (i) includes each of these grain rotations, and is found, as before, from equations (1) and (4):

$$\begin{aligned}&F(\omega_A,\omega_B,\omega_C) \\ &= \frac{1}{\omega_s^3} + \frac{1}{\omega_s^2}\Bigg\{\sum_{n=1}^{\infty} a_n[\cos(kn\omega_A)+\cos(kn\omega_B)+\cos(kn\omega_C)] \\ &\quad + b_n[\sin(kn\omega_A)+\sin(kn\omega_B)+\sin(kn\omega_C)]\Bigg\} \\ &\quad + \frac{1}{\omega_s}\Bigg\{\sum_{m=1}^{\infty}\sum_{n=1}^{\infty}[a_m\cos(km\omega_A)+b_m\sin(km\omega_A)] \\ &\quad \times [a_n\cos(kn\omega_B)+b_n\sin(kn\omega_B)] \\ &\quad + [a_m\cos(km\omega_B)+b_m\sin(km\omega_B)] \\ &\quad \times [a_n\cos(kn\omega_C)+b_n\sin(kn\omega_C)] \\ &\quad + [a_m\cos(km\omega_C)+b_m\sin(km\omega_C)] \\ &\quad \times [a_n\cos(kn\omega_A)+b_n\sin(kn\omega_A)]\Bigg\} \\ &\quad + \Bigg\{\sum_{j=1}^{\infty}\sum_{m=1}^{\infty}\sum_{n=1}^{\infty}[a_j\cos(kj\omega_A)+b_j\sin(kj\omega_A)] \\ &\quad \times [a_m\cos(km\omega_B)+b_m\sin(km\omega_B)] \\ &\quad \times [a_n\cos(kn\omega_C)+b_n\sin(kn\omega_C)]\Bigg\}.\end{aligned}\tag{16}$$

Transformation from a distribution of grain rotations to one of misorientations requires a description of the misorientations in terms of the grain rotations, as in step (ii). This appears in the form

$$\begin{pmatrix}\theta_A\\ \theta_B\\ \theta_C\end{pmatrix} = \begin{pmatrix}0 & -1 & 1\\ 1 & 0 & -1\\ -1 & 1 & 0\end{pmatrix}\begin{pmatrix}\omega_A\\ \omega_B\\ \omega_C\end{pmatrix}, \tag{17}$$

derived by use of equation (2). Regrettably, the transformation matrix $\boldsymbol{A}$ is not invertible due to the linear dependence of the misorientations; a Frank–Nabarro circuit around the triple junction must start and finish in material of the same orientation, implying that the combination of the misorientations accumulated from grain to grain must be described by the identity operation (Frary & Schuh, 2003*a*). Given two rotations, this constraint uniquely specifies the third. Since $\boldsymbol{A}$ is not invertible, we resort to singular-value decomposition and piecewise application of the transformation components to perform steps (iii) and (iv), as outlined in Appendix B. This provides the probability distribution function

$$
\begin{aligned}
&F(\theta_A, \theta_B, \theta_C) \\
&= \left(\frac{\sqrt{3}}{3\omega_s^2} + \frac{\sqrt{3}}{6} \left\{ \sum_{n=1}^{\infty} (a_n^2 + b_n^2)[\cos(kn\theta_A) + \cos(kn\theta_B) \right.\right. \\
&\quad \left.\left. + \cos(kn\theta_C)] \right\} + \frac{\sqrt{3}\omega_s}{12} \left\{ \sum_{m=1}^{\infty} \sum_{n=1}^{\infty} [a_{m+n}(a_m a_n - b_m b_n) \right. \\
&\quad + b_{m+n}(a_n b_m + a_m b_n)][\cos(km\theta_A - kn\theta_B) \\
&\quad + \cos(km\theta_B - kn\theta_C) + \cos(km\theta_C - kn\theta_A)] \\
&\quad - [a_{m+n}(a_n b_m + a_m b_n) - b_{m+n}(a_m a_n - b_m b_n)] \\
&\quad \times [\sin(km\theta_A - kn\theta_B) + \sin(km\theta_B - kn\theta_C) \\
&\quad \left. + \sin(km\theta_C - kn\theta_A)] \right\} \Bigg) \delta(\theta_A + \theta_B + \theta_C). \qquad (18)
\end{aligned}
$$

Our definitions of θ_A, θ_B and θ_C require that each one display an independent periodicity of period ω_s, as represented by the cubic lattice and cubic unit cell in Fig. 5(*a*). To perform step (v) and satisfy this requirement, we must initially determine the periodicity of F. As above, ω_A, ω_B and ω_C are symmetrically equivalent with $\omega_A + j\omega_s$, $\omega_B + m\omega_s$ and $\omega_C + n\omega_s$, respectively, where j, m and n are integers. From equation (17), this implies the symmetric equivalence of θ_A, θ_B and θ_C with $\theta_A + \omega_s(-m + n)$, $\theta_B + \omega_s(j - n)$ and $\theta_C + \omega_s(-j + m)$, respectively. Systematically varying the allowed values of j, m and n results in a lattice of symmetrically equivalent points in the (1, 1, 1) plane, *i.e.* the $\theta_A + \theta_B + \theta_C = 0$ plane, as displayed in Fig. 5(*b*). Examination of these figures indicates that the lattice in Fig. 5(*a*) may be constructed by imposing the necessary infinite translational symmetry on the lattice in Fig. 5(*b*), or

$$
\mathscr{F}(\theta_A, \theta_B, \theta_C) = \sum_{-\infty}^{\infty} F(\theta_A, \theta_B, \theta_C + n\omega_s). \qquad (19)
$$

Practically speaking, though, $\mathscr{F}$ need only include those terms that contribute probability density to the unit cell centred about the origin. Since the terms of equation (19) represent distributions on parallel (1, 1, 1) planes, only those planes that pass through the cubic unit cell of edge length ω_s centred on the origin need be retained. Only three of the planes included in equation (19) satisfy this condition, reducing the expression for $\mathscr{F}$ to

$$
\begin{aligned}
\mathscr{F}(\theta_A, \theta_B, \theta_C) = {} & F(\theta_A, \theta_B, \theta_C - \omega_s) + F(\theta_A, \theta_B, \theta_C) \\
& + F(\theta_A, \theta_B, \theta_C + \omega_s), \qquad (20)
\end{aligned}
$$

giving the joint distribution function for the misorientations around a triple junction, for arbitrary textures described by equation (1).

5. Derived quantities

In order to better appreciate the correlations in grain-boundary networks, the full information content of the distributions $\mathscr{F}$ may be reduced to a few easily understood parameters by applying a classification criterion to separate the boundaries into discrete types. Although any classification scheme dependent on the boundary misorientation may be used with the above distributions, we restrict ourselves to two types of quantities appearing frequently in the literature pertaining to this problem. These are the special fraction p – the fraction of boundaries within the networks whose disorientation falls below a threshold value θ_t – and the triple-junction fractions J_3, J_2, J_1 and J_0 – the fractions of triple junctions coordinated by the subscripted number of special boundaries. In this section, we derive these quantities from equation (13) and equation (20), respectively.

5.1. Special fraction

The fraction of boundaries with a disorientation less than the threshold angle θ_t is given by the integral

$$
p = \int_{-\theta_t}^{\theta_t} \mathscr{F}(\theta)\, \mathrm{d}\theta \qquad (21)
$$

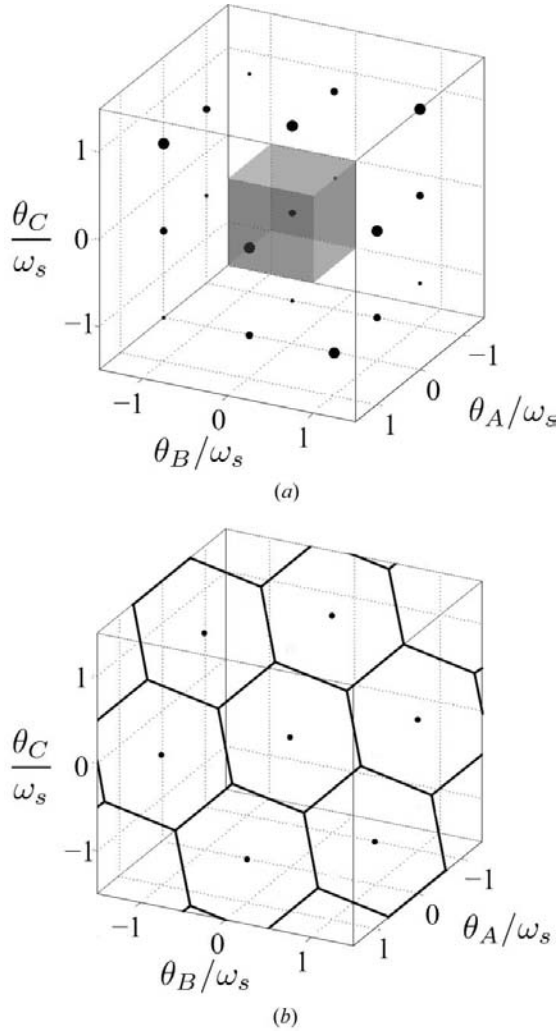

Figure 5
Lattices of symmetrically equivalent points and corresponding unit cells for θ_A, θ_B and θ_C at a triple junction. (*a*) θ_A, θ_B and θ_C each display independent periodicities of ω_s, resulting in a cubic lattice. The size of the markers indicates the relative positions of points residing in the three (1, 1, 1)-type planes shown. (*b*) The three misorientations display joint periodicities, such that the lattice resides entirely in the (1, 1, 1) plane and each lattice point satisfies the constraint $\theta_A + \theta_B + \theta_C = 0$.

with the constraint that $0 \leq \theta_t < \omega_s/2$, since this spans the unique range of the disorientation θ. Performing this integral using equation (13) for $\mathscr{F}(\theta)$ gives

$$p = \frac{2\theta_t}{\omega_s} + \frac{\omega_s^2}{2\pi}\sum_{n=1}^{\infty}\frac{1}{n}(a_n^2 + b_n^2)\sin(kn\theta_t). \quad (22)$$

5.2. Triple-junction fractions

Determining the fractions of triple junctions is rather more involved, since the joint distribution of misorientations around a triple junction must be manipulated rather than the distribution of a single misorientation. The steps required to determine the triple-junction populations are the following.

(i) Specify the disorientation θ_t that separates the low disorientation special boundaries from the high disorientation general boundaries. θ_t is by definition unsigned, and must fall within the range $0 \leq \theta_t < \omega_s/2$.

(ii) Classify every region within the fundamental zone of the joint misorientation distribution in terms of the number of misorientations θ_A, θ_B and θ_C in that region smaller in magnitude than the threshold disorientation θ_t. Within a particular region, this provides the number of special boundaries coordinating a given triple junction, or equivalently the subscript of the triple-junction fraction to which probability density falling within this region contributes. An example of this classification is performed for equation (20) in Fig. 6(*a*) and for equation (18) in Fig. 6(*b*) for the case of $0 \leq \theta_t < \omega_s/3$, where white regions containing no special boundaries contribute to J_0, and the three successive shades of grey contribute to J_1, J_2 and J_3, respectively.

(iii) Integrate the surface distribution function over the ranges specified above and construct the triple-junction fractions by summing the results from regions of the same special boundary coordination. Integration over a single region is performed by parameterizing the surface in θ_A and θ_B, or

$$\int_S \mathscr{F}(\mathbf{y})\,\mathrm{d}A = \iint_T \mathscr{F}(\mathbf{y}(\theta_A,\theta_B))\left|\frac{\partial \mathbf{y}}{\partial \theta_A} \times \frac{\partial \mathbf{y}}{\partial \theta_B}\right| \mathrm{d}\theta_A\,\mathrm{d}\theta_B, \quad (23)$$

where $\mathbf{y} = \theta_A\mathbf{y}_1 + \theta_B\mathbf{y}_2 + \theta_C\mathbf{y}_3$ is expressed as a function of θ_A and θ_B alone using the equation of the surface, $\theta_A + \theta_B + \theta_C = 0$. The magnitude of the cross product of the partial derivatives of $\mathbf{y}$ appearing in equation (23) is a numerical factor related to the ratio of a unit surface area to the projected area in the plane spanned by θ_A and θ_B and, in this case, is a constant equal to $\sqrt{3}$.

For the sake of brevity, we omit the equations for the boundaries of the regions within the fundamental zone, as well as the integral equations leading to the derivation of the triple-junction fractions. The final results of this analysis appear in Appendix *C*, where we present a complete analytical solution for the triple-junction distribution for arbitrary texture functions. The reader will notice that these expressions satisfy several physically necessary constraints; for example, since every triple junction must be one of J_3, J_2, J_1 or J_0, the sum of these quantities must be unity, or

$$J_3 + J_2 + J_1 + J_0 = 1. \quad (24)$$

A further constraint arises when each boundary in the system may be uniquely assigned to a single triple junction, namely, that the triple-junction fractions must be consistent with the fraction of special boundaries around that junction, *i.e.*

$$J_3 + 2J_2/3 + J_1/3 = p. \quad (25)$$

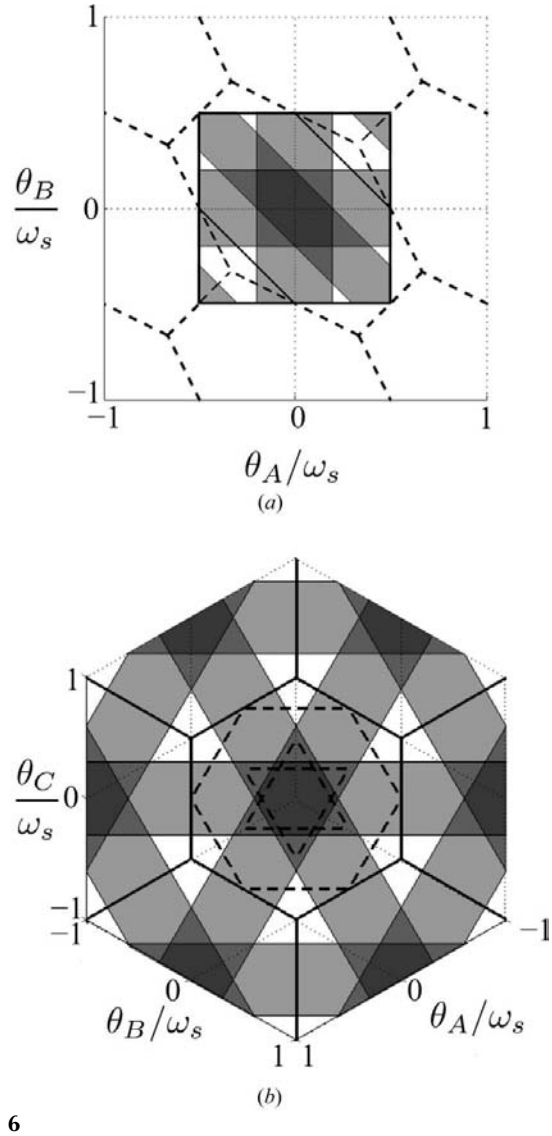

Figure 6
Representation of the distribution functions for misorientations about a triple junction. Triple junctions are classified by the number of misorientations smaller in magnitude than θ_t; for this figure, $0 \leq \theta_t < \omega_s/3$. Darker shading corresponds to more special boundaries, *e.g.* white is a J_0 region and dark grey is a J_3 region. Solid lines indicate unit-cell borders in the current representation and dashed lines in the alternative representation. (*a*) Classification of triple junctions as defined by equation (20). For clarity of representation, the distribution is projected into the plane spanned by θ_A and θ_B. This representation is preferred for integration due to the simplicity of the equations of the region boundaries. (*b*) Classification of the triple-junction distribution defined by equation (18). Bands of special boundaries occur in a high-symmetry configuration, and classification is continued outside the fundamental zone to emphasize this symmetry. The three regions in dashed lines correspond to the three parallel planes that intersect the unit cell appearing in Fig. 5(*a*).

6. Comparison with prior literature

The majority of investigations into correlated grain boundary structures consider two-dimensional networks similar to our system (Schuh, Minich & Kumar, 2003; Frary & Schuh, 2003*b*, 2004, 2005*a*,*b*; Schuh & Frary, 2006; Van Siclen, 2006); this restriction is due principally to the complexity of the three-dimensional case. Of these, only the works of Frary & Schuh (2004) and Van Siclen (2006) provide analytical solutions for the special fraction and triple-junction fractions of correlated networks. The present solution is exact for arbitrary two-dimensional polycrystals, and therefore more general as compared with these studies. When specific simplifying assumptions are used, the results of Frary & Schuh (2004) and Van Siclen (2006) can be recovered. In this section, we demonstrate agreement with their results by simplifying our expression for the special fraction to a form that corresponds with their solutions, and further by numerical evaluation and comparison of triple-junction fractions.

6.1. Simplification for sharp textures

Our decision to represent $f(\omega)$ in equation (1) as a Fourier series allows us to predict grain-boundary character distributions for arbitrary orientation distribution functions, and naturally captures the effect of the k-fold rotational axis consistent with any chosen crystal symmetry. For certain situations, the above distributions may be converted to integrals, and potentially evaluated to provide simple closed-form expressions. The necessary, though not sufficient, conditions for this to be done while maintaining accurate distributions are:

(i) a closed-form analytic expression for $f(\omega)$, the orientation distribution function, exists and is readily available;

(ii) the texture is sufficiently sharp that any distributions of probability density arising from symmetrically equivalent points do not impinge on the fundamental zone of the distribution being converted.

As an example of the procedure, we shall convert the orientation distribution function in equation (1) to integral form. By condition (i), the Fourier coefficients may be calculated as analytic functions of n; that is, a_n and b_n in equation (1) may be expressed as $a(n)$ and $b(n)$, respectively. This allows the Fourier-series representation of the orientation distribution function to be written as

$$f(\omega) = \frac{k}{2\pi} + \sum_{n=1}^{\infty} \{a(n)\cos(kn\omega) + b(n)\sin(kn\omega)\}\Delta n, \quad (26)$$

where Δn is the difference in magnitude of successive values of n, in this case unity. We then perform the substitution $kn = m$, giving the equation

$$f(\omega) = \frac{k}{2\pi} + \sum_{m=k}^{\infty} \left[\frac{1}{k} a\left(\frac{m}{k}\right)\cos(m\omega) + \frac{1}{k} b\left(\frac{m}{k}\right)\sin(m\omega)\right]\Delta m, \quad (27)$$

where m is an integer multiple of k. Now, allow the period of the function to approach infinity or, equivalently, allow k to approach arbitrarily small values. While this effectively removes any symmetrically equivalent points, the distribution within the fundamental zone of $-\omega_s/2 \le \omega < \omega_s/2$ remains unchanged by condition (ii). Δm, of magnitude k, becomes a differential quantity, and $f'(\omega) = \lim_{k\to 0} f(\omega)$ becomes the integral

$$f'(\omega) = \int_0^{\infty} a'(n)\cos(n\omega) + b'(n)\sin(n\omega)\,\mathrm{d}n, \quad (28)$$

where the index m is relabelled as n, and we define $a'(n)$ and $b'(n)$ in terms of the Fourier coefficients $a(n)$ and $b(n)$ as $a'(n) = \lim_{k\to 0} a(n/k)/k$ and $b'(n) = \lim_{k\to 0} b(n/k)/k$. The existence of non-zero values of $a'(n)$ and $b'(n)$ for some value of n is implied by the normalization of $f(\omega)$, *i.e.* that $f'(\omega)$ is non-zero somewhere in the range $-\omega_s/2 \le \omega < \omega_s/2$. Notice that neither k nor ω_s appear explicitly in equation (28); by removing all symmetrically equivalent points, the distribution function is made independent of crystal symmetry.

Although the above example is circular, deriving an integral form for $f'(\omega)$ given the existence and availability of a closed-form analytical expression for $f(\omega)$, the utility of this procedure lies in the ability to derive integral forms for other distribution functions in terms of $a'(n)$ and $b'(n)$. For instance, applying this procedure to equation (22) gives an expression for the special fraction of the network:

$$p' = 2\pi \int_0^{\infty} [a'(n)^2 + b'(n)^2]\frac{1}{n}\sin(n\theta_t)\,\mathrm{d}n, \quad (29)$$

where the prime symbol denotes quantities derived for sharp textures. Comparison of this result with the expressions provided by Frary & Schuh or Van Siclen requires the evaluation of equation (29) using the Fourier coefficients that describe their orientation distribution functions. Since they define ω to be uniformly distributed on the interval $-\omega_{\max} \le \omega < \omega_{\max}$, the appropriate Fourier coefficients are

$$a(n) = \frac{1}{\pi n \omega_{\max}}\sin(kn\omega_{\max}), \quad b(n) = 0. \quad (30)$$

Evaluation and simplification of equation (29) using these Fourier coefficients provides the piecewise function

$$p' = \begin{cases} 1, & 0 \le \omega_{\max} < \theta_t/2 \\ \dfrac{\theta_t}{\omega_{\max}} - \frac{1}{4}\left(\dfrac{\theta_t}{\omega_{\max}}\right)^2, & \theta_t/2 < \omega_{\max}, \end{cases} \quad (31)$$

which is quite similar to the results in the literature. For comparison, our equation (22) and the simplified equation (31) appear along with the solutions by Frary & Schuh (2004) and Van Siclen (2006) in Fig. 7.

The three regions of Fig. 7 separated by vertical dashed lines correspond to three distinct physical situations, and are identifiable by considering the limiting values of the misorientation. Equation (2) and the orientation distribution function reveal that misorientations exist only from $-2\omega_{\max}$ to $2\omega_{\max}$, or equivalently within $2\omega_{\max}$ of any of the symmetrically equivalent points occurring at integer multiples of ω_s. For sharp textures where $2\omega_{\max}$ is smaller than the

threshold disorientation θ_t, or $0 \leq \omega_{max} < \theta_t/2$, every boundary in the network is special. The upper limit of this region is denoted by the vertical dashed line at small values of ω_{max}. For weak textures, the distributions centred on other multiples of ω_s begin to contribute to the probability that a misorientation is smaller than θ_t, and the symmetry of the crystal influences the special fraction. This occurs when $\omega_s - 2\omega_{max}$ is less than θ_t, or for $\omega_s/2 - \theta_t/2 < \omega_{max}$; the lower bound of the region is denoted by the vertical dashed line at higher values of ω_{max}.

Frary & Schuh (2004) and Van Siclen (2006) separately derived the expression for p shown by the dashed grey line in Fig. 7. This solution is accurate for $\theta_t/2 \leq \omega_{max} < \omega_s/2 - \theta_t/2$, and within this range the special fraction is independent of crystal symmetry exactly as claimed by Frary & Schuh (2004). However, Frary & Schuh as well as Van Siclen neglected the component of the piecewise solution for $\omega_{max} < \theta_t/2$, which equation (31) includes. Furthermore, neither the solution by Frary & Schuh and Van Siclen nor equation (31) consider contributions from symmetrically equivalent distributions, and hence deviate from the crystallographically consistent special fraction for $\omega_s/2 - \theta_t/2 < \omega_{max}$. Van Siclen acknowledged this, and with an independent calculation found the value of the special fraction for $\omega_{max} = \omega_s/2$ or, in his terminology, for an isotropic polycrystal (Van Siclen, 2006). Notice that our exact solution, expressed in equation (22) and given in Fig. 7 by the dark solid line, is physically reasonable for $0 \leq \omega_{max} < \omega_s/2 - \theta_t/2$, incorporates the effects of crystal symmetry for $\omega_s/2 - \theta_t/2 < \omega_{max}$, and includes the result provided by Van Siclen for an isotropic crystal.

6.2. Numerical evaluation of triple-junction fractions

Triple-junction fractions contain significant information about the structure of special boundary clusters; in particular, the presence or absence of J_2 junctions in a boundary network influences the fraction of special boundaries necessary to develop a percolating cluster (Frary & Schuh, 2004), and presumably affects a variety of intergranular phenomena. Frary & Schuh (2004) and Van Siclen (2006) developed closed-form analytical solutions for the triple-junction fractions with an orientation distribution function distributed uniformly on the interval $-\omega_{max} \leq \omega < \omega_{max}$. The results of these authors for $0 \leq \omega_{max} < \omega_s/2 - \theta_t/2$ are identical and appear in Fig. 8 as the dark solid line. A second solution found by Van Siclen for $\omega_{max} = \omega_s/2$ is denoted by the heavy dashed line. For comparison, the fractions in a random polycrystal without crystallographic consistency are given as dotted lines. Imposing the requirement of crystallographic consistency

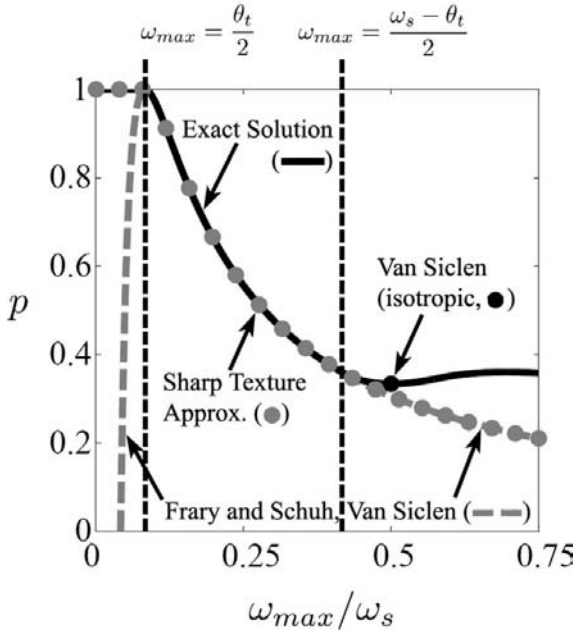

Figure 7
Analytical solutions for the special fraction of boundaries in correlated boundary networks, for the specific case where ω is uniformly distributed on the interval $-\omega_{max} \leq \omega < \omega_{max}$ and $\theta_t = \omega_s/6$ with ω_s the angle of rotational symmetry of the crystallites. Our exact solution [equation (22)] is given by the solid black line and is valid over the full range of ω_{max}/ω_s. The vertical dashed lines appear at $\omega_{max} = \theta_t/2$ and $\omega_{max} = \omega_s/2 - \theta_t/2$. The solutions of Frary & Schuh (2004) and Van Siclen (2006) are represented by the dashed grey line, which deviates for $\omega_{max} < \theta_t/2$ and excludes the effects of crystal symmetry for $\omega_s/2 - \theta_t/2 < \omega_{max}$. A further result for $\omega_{max} = \omega_s/2$, found by Van Siclen, is denoted by the black dot. Equation (31), our simplification for sharp textures, is shown by the series of grey points.

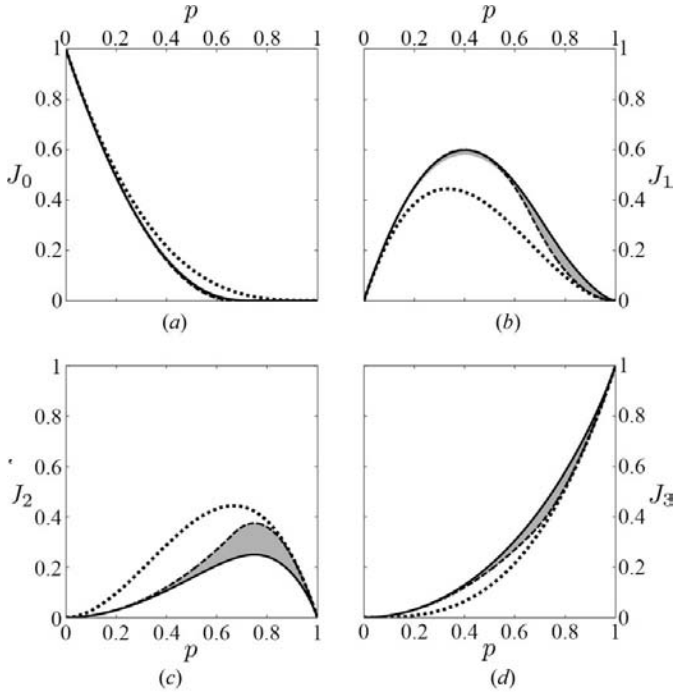

Figure 8
Triple-junction fractions plotted as a function of the special boundary fraction in correlated boundary networks, for the specific case where ω is distributed uniformly on the interval $-\omega_{max} \leq \omega < \omega_{max}$. For comparison, the dotted lines show the predicted triple-junction fractions for a random (uncorrelated) spatial distribution of misorientations. Solutions by Frary & Schuh (2004) and Van Siclen (2006) for $\omega_{max} < \omega_s/2 - \theta_t/2$ appear as the solid lines, and the specific case derived by Van Siclen for $\omega_{max} = \omega_s/2$ is given by the dashed lines. Our solutions, presented in Appendix *C*, migrate continuously over the regions shaded in grey with changes in the values of ω_s and θ_t.

clearly affects the triple-junction fractions and, through them, the topology of the boundary network.

For comparison with our results, we use the Fourier coefficients of equation (30) to numerically evaluate the equations presented in Appendix *C*. By independently varying the threshold disorientation θ_t over $0 \leq \theta_t < \omega_s/2$ and $\omega_{\max}$ over $0 \leq \omega_{\max} < 2\omega_s$, we find a continuous range of allowable triple-junction fractions, shown in Fig. 8 as the shaded grey region. Although Frary & Schuh and Van Siclen developed equations within the allowable range of values, they do not describe the boundaries of our results. While this subtle effect is difficult to see in Fig. 8, our results for this specific texture include those of Frary & Schuh (2004) and Van Siclen (2006), the transitional solutions between theirs, and further allowable triple-junction fractions outside their equations.

7. Conclusions

The analysis of correlations in grain-boundary distributions is critical to understanding intergranular and transgranular phenomena, and is presumably of interest for those investigating any material behaviour strongly affected by boundary character. Our contribution in this paper is an analytical method to describe and determine correlations in grain-boundary character arising solely from the requirement for crystallographic consistency in polycrystals with uncorrelated grain orientations. For the specific case of two-dimensional or two-dimensionally textured polycrystals, we present an exact solution for the misorientation correlations at triple junctions. Extension of the method to more complex structures, *e.g.* grain clusters of more than three boundaries, quadruple nodes in three-dimensional structures with the required texture *etc.*, is possible using the same approach. Our results differ from prior analytical work along these lines in a few respects. Most notably, our expression of distribution functions as Fourier series provides a general solution equally pertinent to all allowed textures and crystal systems, thereby avoiding the necessity of lengthy derivations for individual instances. Furthermore, the prior literature almost exclusively examines correlations in *classification* of boundaries arising from the granular nature of the material, particularly in terms of the triple-junction fractions of 'special' and 'general' boundaries. Our analysis instead considers correlations among the *quantities* describing the boundaries, *e.g.* misorientation angles. This allows classification to be performed as a distinct secondary step, and thereby clarifies the nature and extent of correlations in the structure.

APPENDIX *A*
Definite trigonometric integrals

Integration of texture functions expressed using the Fourier-series representation generally requires integration of trigonometric terms over intervals corresponding to a single period. The values of these definite integrals may be found by expansion of the trigonometric terms as complex exponentials, followed by evaluation of the integral of each exponential independently. A reference for integrals of trigonometric terms used in this paper follows, omitting the integrals of odd functions, which vanish:

$$\int_{-\pi}^{\pi} \cos(nx)\,\mathrm{d}x = 0 \tag{32}$$

$$\int_{-\pi}^{\pi} \cos(mx)\cos(nx)\,\mathrm{d}x = \pi\delta_{mn} \tag{33}$$

$$\int_{-\pi}^{\pi} \sin(mx)\sin(nx)\,\mathrm{d}x = \pi\delta_{mn} \tag{34}$$

$$\int_{-\pi}^{\pi} \cos(jx)\cos(mx)\cos(nx)\,\mathrm{d}x = \frac{\pi}{2}(\delta_{m+n,j} + \delta_{j+n,m} + \delta_{j+m,n}) \tag{35}$$

$$\int_{-\pi}^{\pi} \cos(jx)\sin(mx)\sin(nx)\,\mathrm{d}x = \frac{\pi}{2}(-\delta_{m+n,j} + \delta_{j+n,m} + \delta_{j+m,n}), \tag{36}$$

where the indices j, m and n are positive integers and δ is the Kronecker delta.

APPENDIX *B*
Singular-value decomposition

The matrix $\boldsymbol{A}$ in equation (17) is not invertible due to the dependence of the misorientations as derived from physical arguments. Performing singular-value decomposition on $\boldsymbol{A}$ results in the factorization

$$\begin{aligned}\boldsymbol{A} &= \boldsymbol{U}\boldsymbol{\Sigma}\boldsymbol{V}^T \\ &= \begin{pmatrix} 1/\sqrt{6} & -1/\sqrt{2} & 1/\sqrt{3} \\ 1/\sqrt{6} & 1/\sqrt{2} & 1/\sqrt{3} \\ -2/\sqrt{6} & 0 & 1/\sqrt{3} \end{pmatrix} \begin{pmatrix} \sqrt{3} & 0 & 0 \\ 0 & \sqrt{3} & 0 \\ 0 & 0 & 0 \end{pmatrix} \\ &\quad \times \begin{pmatrix} 1/\sqrt{2} & -1/\sqrt{2} & 0 \\ 1/\sqrt{6} & 1/\sqrt{6} & -2/\sqrt{6} \\ 1/\sqrt{3} & 1/\sqrt{3} & 1/\sqrt{3} \end{pmatrix},\end{aligned} \tag{37}$$

where the transformation $\boldsymbol{A}$ is expressed in terms of an orthogonal matrix $\boldsymbol{V}$, a matrix $\boldsymbol{\Sigma}$ that contains the singular values of $\boldsymbol{A}$ and performs a stretching of space, and a further orthogonal matrix $\boldsymbol{U}$; a single transformation $\boldsymbol{A}$ is now replaced by three component transformations. The columns of $\boldsymbol{V}$ and $\boldsymbol{U}$ form orthonormal bases for the $\boldsymbol{\omega}$ and $\mathbf{y}$ spaces, respectively.

We now consider these transformations in order. The initial component of the desired transformation in equation (37) is a change in coordinates from ω_A, ω_B and ω_C to v_1, v_2 and v_3, the columns of $\boldsymbol{V}$. This transformation is performed by the matrix $\boldsymbol{V}^T$, and is given explicitly by

$$\begin{pmatrix} v_1 \\ v_2 \\ v_3 \end{pmatrix} = \begin{pmatrix} 1/\sqrt{2} & -1/\sqrt{2} & 0 \\ 1/\sqrt{6} & 1/\sqrt{6} & -2/\sqrt{6} \\ 1/\sqrt{3} & 1/\sqrt{3} & 1/\sqrt{3} \end{pmatrix} \begin{pmatrix} \omega_A \\ \omega_B \\ \omega_C \end{pmatrix}. \quad (38)$$

Inversion of this equation provides the relations $\omega_A = v_1/\sqrt{2} + v_2/\sqrt{6} + v_3/\sqrt{3}$, $\omega_B = -v_1/\sqrt{2} + v_2/\sqrt{6} + + v_3/\sqrt{3}$ and $\omega_C = -2v_2/\sqrt{6} + v_3/\sqrt{3}$. Since $\boldsymbol{V}$ is an orthogonal matrix, the distribution will remain normalized during direct substitution of the above equalities into equation (16); this completes one component of the transformation $\boldsymbol{A}$.

The remaining components of the transformation $\boldsymbol{A}$ appear as

$$\begin{pmatrix} \theta_A \\ \theta_B \\ \theta_C \end{pmatrix} = \begin{pmatrix} 1/\sqrt{6} & -1/\sqrt{2} & 1/\sqrt{3} \\ 1/\sqrt{6} & 1/\sqrt{2} & 1/\sqrt{3} \\ -2/\sqrt{6} & 0 & 1/\sqrt{3} \end{pmatrix} \times \begin{pmatrix} \sqrt{3} & 0 & 0 \\ 0 & \sqrt{3} & 0 \\ 0 & 0 & 0 \end{pmatrix} \begin{pmatrix} v_1 \\ v_2 \\ v_3 \end{pmatrix}. \quad (39)$$

Examination of $\boldsymbol{\Sigma}$ reveals that the null space of the transformation $\boldsymbol{A}$ is spanned by a unit vector pointing along v_3; the dependence of $F(v_1, v_2, v_3)$ on this quantity must be removed by integration before the remaining transformation may proceed. To determine the limits of integration, recall the symmetric equivalence of ω_A, ω_B and ω_C with $\omega_A + j\omega_s$, $\omega_B + m\omega_s$ and $\omega_C + n\omega_s$, respectively, where j, m and n are integers. From equation (38), this implies the symmetric equivalence of v_1, v_2 and v_3 with $v_1 + (j - m)\omega_s/\sqrt{2}$, $v_2 + (j + m - 2n)\omega_s/\sqrt{6}$ and $v_3 + (j + m + n)\omega_s/\sqrt{3}$, respectively. Notice that setting the values of j, m and n each to unity shifts the value of v_3 by the smallest amount that simultaneously leaves the values of v_1 and v_2 invariant; hence, the distribution is periodic in v_3 with a period of $\sqrt{3}\omega_s$, and the dependence on v_3 may be removed by integrating over this range. The appropriate integral is therefore

$$F(v_1, v_2) = \int_{-\sqrt{3}\omega_s/2}^{\sqrt{3}\omega_s/2} F(v_1, v_2, v_3)\, \mathrm{d}v_3. \quad (40)$$

Performing this integral, with reference to the integrals of trigonometric functions in Appendix A allows the joint distribution function of v_1 and v_2 to be expressed by

$$\begin{aligned} F(v_1, v_2) = {} & \frac{\sqrt{3}}{\omega_s^2} + \frac{\sqrt{3}}{2}\left(\sum_{n=1}^{\infty} (a_n^2 + b_n^2) \left\{ \cos(\sqrt{2}knv_1) \right.\right. \\ & + \cos\left[\frac{\sqrt{2}k}{2} n(v_1 + \sqrt{3}v_2) \right] \\ & \left.\left. + \cos\left[\frac{\sqrt{2}k}{2} n(v_1 - \sqrt{3}v_2) \right] \right\} \right) \\ & + \frac{\sqrt{3}\omega_s}{4}\left(\sum_{m=1}^{\infty} \sum_{n=1}^{\infty} [a_{m+n}(a_m a_n - b_m b_n) \right. \\ & + b_{m+n}(a_n b_m + a_m b_n)] \\ & \times \left\{ \cos\left[\sqrt{2}kmv_1 + \frac{\sqrt{2}k}{2} n(v_1 + \sqrt{3}v_2) \right] \right. \\ & + \cos\left[\sqrt{2}kmv_1 + \frac{\sqrt{2}k}{2} n(v_1 - \sqrt{3}v_2) \right] \\ & \left. + \cos\left[\frac{\sqrt{2}k}{2} m(v_1 + \sqrt{3}v_2) - \frac{\sqrt{2}k}{2} n(v_1 - \sqrt{3}v_2) \right] \right\} \\ & + [a_{m+n}(a_n b_m + a_m b_n) - b_{m+n}(a_m a_n - b_m b_n)] \\ & \times \left\{ - \sin\left[\sqrt{2}kmv_1 + \frac{\sqrt{2}k}{2} n(v_1 + \sqrt{3}v_2) \right] \right. \\ & + \sin\left[\sqrt{2}kmv_1 + \frac{\sqrt{2}k}{2} n(v_1 - \sqrt{3}v_2) \right] \\ & \left.\left. + \sin\left[\frac{\sqrt{2}k}{2} m(v_1 + \sqrt{3}v_2) - \frac{\sqrt{2}k}{2} n(v_1 - \sqrt{3}v_2) \right] \right\} \right). \end{aligned} \quad (41)$$

At this point, the remaining v_1 and v_2 must be found in terms of the misorientations θ_A, θ_B and θ_C. Our procedure is similar to the construction of the pseudoinverse $\boldsymbol{A}^+$, as explained in, for example, Strang (2006). Recall the decomposition of $\boldsymbol{A}$ and the subsequent completion of the transformation $\boldsymbol{V}^T$; this situation is expressed mathematically by

$$\mathbf{y} = \boldsymbol{A}\boldsymbol{\omega} = \boldsymbol{U}\boldsymbol{\Sigma}\boldsymbol{V}^T\boldsymbol{\omega} = \boldsymbol{U}\boldsymbol{\Sigma}\mathbf{v}. \quad (42)$$

Left multiplication of the sides of this equation by $\boldsymbol{U}^T$ and $\boldsymbol{\Sigma}^+$, defined as the matrix $\boldsymbol{\Sigma}^T$ with the non-zero diagonal values inverted, provides the equation

$$\boldsymbol{\Sigma}^+\boldsymbol{U}^T\mathbf{y} = \boldsymbol{\Sigma}^+\boldsymbol{U}^T\boldsymbol{U}\boldsymbol{\Sigma}\mathbf{v} = \boldsymbol{\Sigma}^+\boldsymbol{\Sigma}\mathbf{v}, \quad (43)$$

where $\boldsymbol{U}^T\boldsymbol{U} = \boldsymbol{I}$ since $\boldsymbol{U}$ is orthogonal. Explicit evaluation using the matrices provided in equation (37) gives the matrix equation

$$\begin{pmatrix} \sqrt{2}/6 & \sqrt{2}/6 & -\sqrt{2}/3 \\ -1/\sqrt{6} & 1/\sqrt{6} & 0 \\ 0 & 0 & 0 \end{pmatrix} \begin{pmatrix} \theta_A \\ \theta_B \\ \theta_C \end{pmatrix} = \begin{pmatrix} 1 & 0 & 0 \\ 0 & 1 & 0 \\ 0 & 0 & 0 \end{pmatrix} \begin{pmatrix} v_1 \\ v_2 \\ v_3 \end{pmatrix}, \quad (44)$$

from which $v_1 = \sqrt{2}\theta_A/6 + \sqrt{2}\theta_B/6 - \sqrt{2}\theta_C/3$ and $v_2 = -\theta_A/\sqrt{6} + \theta_B/\sqrt{6}$. An expression for v_3 is not necessary, since integration has already removed the dependence of F on this quantity. Substitution of these equations into equation (41), and multiplication by the product of the non-zero diagonal values of $\boldsymbol{\Sigma}^+$, in this case 1/3, results in the equation

$$
\begin{aligned}
&F(\theta_A,\theta_B,\theta_C)\\
&\quad=\left[\frac{\sqrt{3}}{3\omega_s^2}+\frac{\sqrt{3}}{6}\left(\sum_{n=1}^{\infty}(a_n^2+b_n^2)\left\{\cos\left[\frac{k}{3}n(-2\theta_A+\theta_B+\theta_C)\right]\right.\right.\right.\\
&\qquad+\cos\left[\frac{k}{3}n(\theta_A-2\theta_B+\theta_C)\right]\\
&\qquad\left.\left.\left.+\cos\left[\frac{k}{3}n(\theta_A+\theta_B-2\theta_C)\right]\right\}\right)\right.\\
&\qquad+\frac{\sqrt{3}\omega_s}{12}\left(\sum_{m=1}^{\infty}\sum_{n=1}^{\infty}\left[a_{m+n}(a_ma_n-b_mb_n)\right.\right.\\
&\qquad\left.+b_{m+n}(a_nb_m+a_mb_n)\right]\\
&\qquad\times\left\{\cos\left[\frac{k}{3}m(-2\theta_A+\theta_B+\theta_C)-\frac{k}{3}n(\theta_A-2\theta_B+\theta_C)\right]\right.\\
&\qquad+\cos\left[\frac{k}{3}m(\theta_A-2\theta_B+\theta_C)-\frac{k}{3}n(\theta_A+\theta_B-2\theta_C)\right]\\
&\qquad\left.+\cos\left[\frac{k}{3}m(\theta_A+\theta_B-2\theta_C)-\frac{k}{3}n(-2\theta_A+\theta_B+\theta_C)\right]\right\}\\
&\qquad+[a_{m+n}(a_nb_m+a_mb_n)-b_{m+n}(a_ma_n-b_mb_n)]\\
&\qquad\times\left\{\sin\left[\frac{k}{3}m(-2\theta_A+\theta_B+\theta_C)-\frac{k}{3}n(\theta_A-2\theta_B+\theta_C)\right]\right.\\
&\qquad+\sin\left[\frac{k}{3}m(\theta_A-2\theta_B+\theta_C)-\frac{k}{3}n(\theta_A+\theta_B-2\theta_C)\right]\\
&\qquad\left.\left.+\sin\left[\frac{k}{3}m(\theta_A+\theta_B-2\theta_C)-\frac{k}{3}n(-2\theta_A+\theta_B+\theta_C)\right]\right\}\right)\Bigg]\\
&\qquad\times\delta(\theta_A+\theta_B+\theta_C) \qquad (45)
\end{aligned}
$$

for the joint probability distribution of the misorientations around a triple junction. The Dirac delta function reduces F from a volumetric probability distribution to a surface probability distribution; to understand the appearance of this term, recall that, for a circuit around a triple junction, the combination of the misorientations accumulated from grain to grain must be described by the identity operation. Mathematically, this is expressed in our current system as

$$\theta_A+\theta_B+\theta_C=0. \qquad (46)$$

This requires the allowable sets of misorientations, considered as vectors in **y** space, to contain no component in the direction of the vector [1, 1, 1]. This is actually apparent directly from equation (37); since the column vector of $\boldsymbol{U}$ spanning the left null space, or the subspace unreachable by the transformation $\boldsymbol{A}$, points in this direction, a surface probability density function must result. The constraint expressed by the Dirac delta function allows the expression for $F(\theta_A,\theta_B,\theta_C)$ to be considerably simplified, to the form appearing in equation (18).

APPENDIX C
Triple-junction fractions

Following the procedure outlined in §5.2 provides the equations for the triple-junction fractions J_3, J_2, J_1 and J_0 in terms of the Fourier coefficients a_n and b_n and the threshold angle θ_t. Owing to the disappearance of certain regions and the appearance of others when $\theta_t=\omega_s/3$, the form of the equations depends to a certain extent on the threshold angle. For $0\le\theta_t<\omega_s/3$,

$$
\begin{aligned}
J_3=&\frac{3\theta_t^2}{\omega_s^2}+\frac{3\omega_s^2}{4\pi^2}\left\{\sum_{n=1}^{\infty}\frac{1}{n^2}(a_n^2+b_n^2)[1-\cos(kn\theta_t)\right.\\
&\left.+kn\theta_t\sin(kn\theta_t)]\right\}+\frac{3\omega_s^3}{4\pi^2}\left(\sum_{m=1}^{\infty}\sum_{n=1}^{\infty}\frac{1}{(m+n)m}\right.\\
&\times[a_{m+n}(a_ma_n-b_mb_n)+b_{m+n}(a_nb_m+a_mb_n)]\\
&\left.\times\{\cos(kn\theta_t)-\cos[k(m+n)\theta_t]\}\right) \qquad (47)
\end{aligned}
$$

$$
\begin{aligned}
J_2=&\frac{3\theta_t^2}{\omega_s^2}+\frac{3\omega_s^2}{4\pi^2}\left\{\sum_{n=1}^{\infty}\frac{1}{n^2}(a_n^2+b_n^2)[-2+3\cos(kn\theta_t)\right.\\
&\left.-\cos(2kn\theta_t)+kn\theta_t\sin(kn\theta_t)]\right\}\\
&+\frac{3\omega_s^3}{4\pi^2}\left(\sum_{m=1}^{\infty}\sum_{n=1}^{\infty}\frac{1}{(m+n)m}[a_{m+n}(a_ma_n-b_mb_n)\right.\\
&+b_{m+n}(a_nb_m+a_mb_n)]\\
&\times\{-2\cos(kn\theta_t)+2\cos[k(m+n)\theta_t]\\
&\left.+\cos[k(m-n)\theta_t]-\cos[k(2m+n)\theta_t]\}\right) \qquad (48)
\end{aligned}
$$

$$
\begin{aligned}
J_1=&\frac{3\theta_t(2\omega_s-5\theta_t)}{\omega_s^2}+\frac{3\omega_s^2}{4\pi^2}\left\{\sum_{n=1}^{\infty}\frac{1}{n^2}(a_n^2+b_n^2)[1-3\cos(kn\theta_t)\right.\\
&\left.+2\cos(2kn\theta_t)+n(2\pi-5k\theta_t)\sin(kn\theta_t)]\right\}\\
&+\frac{3\omega_s^3}{4\pi^2}\left(\sum_{m=1}^{\infty}\sum_{n=1}^{\infty}\frac{1}{(m+n)m}[a_{m+n}(a_ma_n-b_mb_n)\right.\\
&+b_{m+n}(a_nb_m+a_mb_n)]\{\cos(kn\theta_t)-\cos[k(m+n)\theta_t]\\
&\left.-2\cos[k(m-n)\theta_t]+2\cos[k(2m+n)\theta_t]\}\right) \qquad (49)
\end{aligned}
$$

$$
\begin{aligned}
J_0=&\frac{(\omega_s-3\theta_t)^2}{\omega_s^2}+\frac{3\omega_s^2}{4\pi^2}\left\{\sum_{n=1}^{\infty}\frac{1}{n^2}(a_n^2+b_n^2)[\cos(kn\theta_t)\right.\\
&\left.-\cos(2kn\theta_t)+n(3k\theta_t-2\pi)\sin(kn\theta_t)]\right\}\\
&+\frac{3\omega_s^3}{4\pi^2}\left(\sum_{m=1}^{\infty}\sum_{n=1}^{\infty}\frac{1}{(m+n)m}[a_{m+n}(a_ma_n-b_mb_n)\right.\\
&+b_{m+n}(a_nb_m+a_mb_n)]\{\cos[k(m-n)\theta_t]\\
&\left.-\cos[k(2m+n)\theta_t]\}\right). \qquad (50)
\end{aligned}
$$

Otherwise, when $\omega_s/3\le\theta_t<\omega_s/2$, the equations

$$J_3 = 1 + \frac{6\theta_t(2\theta_t - \omega_s)}{\omega_s^2} + \frac{3\omega_s^2}{2\pi^2}\left\{\sum_{n=1}^{\infty}\frac{1}{n^2}(a_n^2 + b_n^2)\sin(kn\theta_t) \times [2kn\theta_t - n\pi + \sin(kn\theta_t)]\right\} + \frac{3\omega_s^3}{4\pi^2}\left(\sum_{m=1}^{\infty}\sum_{n=1}^{\infty}\frac{1}{(m+n)m}[a_{m+n}(a_m a_n - b_m b_n) + b_{m+n}(a_n b_m + a_m b_n)]\{\cos(kn\theta_t) - \cos[k(m+n)\theta_t] + \cos[k(m-n)\theta_t] - \cos[k(2m+n)\theta_t]\}\right) \quad (51)$$

$$J_2 = -3 + \frac{6\theta_t(3\omega_s - 4\theta_t)}{\omega_s^2} + \frac{3\omega_s^2}{2\pi^2}\left\{\sum_{n=1}^{\infty}\frac{1}{n^2}(a_n^2 + b_n^2)\sin(kn\theta_t) \times [-4kn\theta_t + 3n\pi - 2\sin(kn\theta_t)]\right\} + \frac{3\omega_s^3}{2\pi^2}\left(\sum_{m=1}^{\infty}\sum_{n=1}^{\infty}\frac{1}{(m+n)m}[a_{m+n}(a_m a_n - b_m b_n) + b_{m+n}(a_n b_m + a_m b_n)]\{-\cos(kn\theta_t) + \cos[k(m+n)\theta_t] - \cos[k(m-n)\theta_t] + \cos[k(2m+n)\theta_t]\}\right) \quad (52)$$

$$J_1 = \frac{3(\omega_s - 2\theta_t)^2}{\omega_s^2} + \frac{3\omega_s^2}{2\pi^2}\left\{\sum_{n=1}^{\infty}\frac{1}{n^2}(a_n^2 + b_n^2)\sin(kn\theta_t) \times [2kn\theta_t - 2n\pi + \sin(kn\theta_t)]\right\} + \frac{3\omega_s^3}{4\pi^2}\left(\sum_{m=1}^{\infty}\sum_{n=1}^{\infty}\frac{1}{(m+n)m}[a_{m+n}(a_m a_n - b_m b_n) + b_{m+n}(a_n b_m + a_m b_n)] \times \{\cos(kn\theta_t) - \cos[k(m+n)\theta_t] + \cos[k(m-n)\theta_t] - \cos[k(2m+n)\theta_t]\}\right) \quad (53)$$

$$J_0 = 0 \quad (54)$$

are used instead.

This work was supported by the US National Science Foundation under contract No. DMR-0346848.

References

Adams, B. L. (1986). *Metall. Mater. Trans. A*, **17**, 2199–2207.
Adams, B. L. (1993). *Mater. Sci. Eng. A*, **166**, 59–66.
Adams, B. L. & Field, D. P. (1992). *Metall. Mater. Trans. A*, **23**, 2501–2513.
Adams, B. L., Wright, S. I. & Kunze, K. (1993). *Metall. Mater. Trans. A*, **24**, 819–831.
Adams, B. L., Zhao, J. & Grimmer, H. (1990). *Acta Cryst.* A**46**, 620–622.
Brandon, D. G. (1966). *Acta Metall.* **14**, 1479–1484.
Bunge, H. J. (1993). *Texture Analysis in Materials Science: Mathematical Methods*, 1st ed. Gottingen: Cuvillier Verlag.
Frary, M. & Schuh, C. A. (2003*a*). *Acta Mater.* **51**, 3731–3743.
Frary, M. & Schuh, C. A. (2003*b*). *Appl. Phys. Lett.* **83**, 3755–3757.
Frary, M. & Schuh, C. A. (2004). *Phys. Rev. B*, **69**, 134115.
Frary, M. & Schuh, C. A. (2005*a*). *Acta Mater.* **53**, 4323–4335.
Frary, M. & Schuh, C. A. (2005*b*). *Philos. Mag.* **85**, 1123–1143.
Gertsman, V. Y. (2001*a*). *Acta Cryst.* A**57**, 369–377.
Gertsman, V. Y. (2001*b*). *Acta Cryst.* A**57**, 649–655.
Gertsman, V. Y. (2002). *Acta Cryst.* A**58**, 155–161.
Gertsman, V. Y., Zhilyaev, A. P., Pshenichnyuk, A. I. & Valiev, R. Z. (1992). *Acta Metall. Mater.* **40**, 1433–1441.
Grimmer, H. (1974). *Acta Cryst.* A**30**, 685–688.
Grimmer, H. (1979). *Scr. Metall.* **13**, 161–164.
Grimmer, H. (1980). *Acta Cryst.* A**36**, 382–389.
Haessner, F., Pospiech, J. & Sztwiertnia, K. (1983). *Mater. Sci. Eng.* **57**, 1–14.
Handscomb, D. C. (1957). *Can. J. Math.* **10**, 85–88.
Hilliard, J. E. (1962). *Trans. Metall. Soc. AIME*, **224**, 1201–1211.
Kumar, M., King, W. E. & Schwartz, A. J. (2000). *Acta Mater.* **48**, 2081–2091.
Kumar, M., Schwartz, A. J. & King, W. E. (2002). *Acta Mater.* **50**, 2599–2612.
Mackenzie, J. K. (1958). *Biometrika*, **45**, 229–240.
Mackenzie, J. K. (1964). *Acta Metall.* **12**, 223–225.
Mackenzie, J. K. & Thomson, M. J. (1957). *Biometrika*, **44**, 205–210.
Minich, R. W., Schuh, C. A. & Kumar, M. (2002). *Phys. Rev. B*, **66**, 052101.
Miyazawa, K., Ito, K. & Ishida, Y. (1996). *Mater. Sci. Forum*, **207–209**, 301–304.
Miyazawa, K., Iwasaki, Y., Ito, K. & Ishida, Y. (1996). *Acta Cryst.* A**52**, 787–796.
Morawiec, A. (1995). *J. Appl. Cryst.* **28**, 289–293.
Morawiec, A. & Field, D. P. (1996). *Philos. Mag.* A**73**, 1113–1130.
Morris, P. R., Zhao, J. W. & Adams, B. L. (1988). *Metall. Mater. Trans. A*, **19**, 2611.
Pan, Y. & Adams, B. L. (1994). *Scr. Metall. Mater.* **30**, 1055–1060.
Philofsky, E. M. & Hilliard, J. E. (1969). *Q. Appl. Math.* **27**, 79–86.
Read, W. & Shockley, W. (1950). *Phys. Rev.* **78**, 275–289.
Reed, B. W. & Kumar, M. (2006). *Scr. Mater.* **54**, 1029–1033.
Roe, R.-J. (1965). *J. Appl. Phys.* **36**, 2024–2031.
Roe, R.-J. (1966). *J. Appl. Phys.* **37**, 2069–2072.
Saylor, D. M., El Dasher, B., Pang, Y., Miller, H. M., Wynblatt, P., Rollett, A. D. & Rohrer, G. S. (2004). *J. Am. Ceram. Soc.* **87**, 724–726.
Saylor, D. M., El Dasher, B. S., Rollett, A. D. & Rohrer, G. S. (2004). *Acta Mater.* **52**, 3649–3655.
Saylor, D. M., El Dasher, B., Sano, T. & Rohrer, G. S. (2004). *J. Am. Ceram. Soc.* **87**, 670–676.
Saylor, D. M., Morawiec, A. & Rohrer, G. S. (2003*a*). *Acta Mater.* **51**, 3663–3674.
Saylor, D. M., Morawiec, A. & Rohrer, G. S. (2003*b*). *Acta Mater.* **51**, 3675–3686.
Schuh, C. A. & Frary, M. (2006). *Scr. Mater.* **54**, 1023–1028.
Schuh, C. A., Kumar, M. & King, W. E. (2003*a*). *Acta Mater.* **51**, 687–700.
Schuh, C. A., Kumar, M. & King, W. E. (2003*b*). *Z. Metallkd.* **94**, 323–328.
Schuh, C. A., Kumar, M. & King, W. E. (2005). *J. Mater. Sci.* **40**, 847–852.
Schuh, C. A., Minich, R. W. & Kumar, M. (2003). *Philos. Mag.* **83**, 711–726.
Strang, G. (2006). *Linear Algebra and its Applications*, 4th ed. Belmont, CA: Thomson, Brooks/Cole.
Van Siclen, C. D. (2006). *Phys. Rev. B*, **73**, 184118.
Warrington, D. H. & Boon, M. (1975). *Acta Metall.* **23**, 599–607.
Zhao, J. W. & Adams, B. L. (1988). *Acta Cryst.* A**44**, 326–336.
Zhao, J. W., Koontz, J. S. & Adams, B. L. (1988). *Metall. Mater. Trans. A*, **19**, 1179–1185.